Asymmetric Operation of Segmented Dual Three-Phase Electric Machines for Improved Cycle Efficiency

Lorenz Schoch
Institute of Electrical Engineering
Karlsruhe Institute of Technology
Karlsruhe, Germany
lorenz.schoch@kit.edu

Miriam Axtmann
Schaeffler Hub for Advanced Research
Schaeffler Technologies AG & Co. KG
Karlsruhe, Germany
miriam.axtmann@schaeffler.com

Johannes Kolb
Schaeffler Hub for Advanced Research
Schaeffler Technologies AG & Co. KG
Karlsruhe, Germany
johannes.kolb@schaeffler.com

Martin Doppelbauer
Institute of Electrical Engineering
Karlsruhe Institute of Technology
Karlsruhe, Germany
martin.doppelbauer@kit.edu

***Abstract*—This paper presents an approach to improve the overall efficiency of permanent magnet synchronous machines (PMSM) in driving cycles without decreasing the power and torque density. The conflict between high torque densities and high efficiency in driving cycles results in the prioritization of one of these goals. To address this conflict, a design of a segmented dual three-phase electric machine (DTEM) is presented. The two three-phase winding systems of the divided segments are fed by independent converters and separately optimized for different operating ranges. The resulting DTEM is characterized by an asymmetric geometry and operation. The magnetic coupling between the systems is investigated. The geometry is optimized with coupled numerical simulation. The overall losses in a driving cycle can be reduced up to $3.6\,\%$ with minor deterioration in torque.**

***Index Terms*—PMSM, Dual Three Phase, Segmentation, Asymmetric Operation**

I. Introduction

The optimization of electric machines for automotive drives has been the subject of research for many years. The design process in general is characterized by a conflict between high torque densities and high efficiency in driving cycles at partial loads. Various strategies focus on one main objective while neglecting the counterpart. This paper proposes an approach to improving the overall cycle efficiency of permanent magnet synchronous machines (PMSM) in dual-three phase systems with distributed windings without decreasing the power and torque density.

DTEM, fed by two independent converters, are investigated. Multiphase electrical machines, especially with six phases, have received an increased attention in the mobility sector, e.g. for automotive or aviation applications over the last years. Various studies show their benefits on reliability during faulty conditions due to redundancy, their ability to reduce torque-ripple or increase the maximum torque [1]–[3]. The overall safety for critical applications is improved. This vindicates the costs of additional power electronics, such as converters and sensors. The presence of two individual winding systems, additional magnetic coupling between the two three-phase systems must be taken into account. Previous research studies of DTEM focus on symmetric operation of two systems with a fixed phase shift of $\alpha = 30\,^\circ$ between them [1]. The resulting magnetomotive force (MMF) lower harmonics are eliminated compared to the three-phase reference [4]. Another design approach of DTEM is to arrange the winding in segments of $90\,^\circ$ spatially, with neighboring segments fed by different converters [5]. The currents of the two machines are in phase, due to a segmentation per pole pair. In this case, the average torque is lower and the torque ripple is higher, compared to a six-phase machine or a DTEM with fixed phase shift [6].

The stator of the presented DTEM is circumferentially segmented into an even number of parts, in this case 4, due to the number of pole pairs. The neighboring segments are each driven by one of the two three-phase systems. The advantages of segmentation are analyzed in the literature [5], [7]. The authors discuss the benefits of two separately fed and spatially segmented machines. The magnetic coupling between the two separate machines in case of faulty conditions is taken into account.

A general approach in designing segmented, asymmetrically operating machines (SAM) is to consider each three-phase system as an individual machine in a first step and optimize the stator geometry for a different objective, e.g. machine 1 (M1) for high torque densities at high loads and machine 2 (M2) for high efficiencies at partial loads. The required torque in each operating point (OP) is loss-optimal distributed between the two machines. A coupled model will be derived, the magnetic coupling is investigated and discussed.

II. Methods and Modeling

A. Asymmetric geometry and operation

The approach presented in this paper is a DTEM with distributed winding, divided into four segments, where the two opposing segments are fed together by one converter. Both converters operate with the same maximum voltage and are supplied by the same DC link. The star points of the two machines (M1, M2) are neither connected to each other, nor to the converter. Figure 1 illustrates the general topology of SAM. Each machine is optimized for a specific operating range. Depending on the OP, the required torque is loss optimal distributed between M1 and M2, with the result of an asymmetrical, electrical operation. In addition, the separated optimization leads to different geometries in the stator for each machine and results in an asymmetrical geometry. The rotor is symmetrical to minimize unbalanced oscillation and will not be investigated in this optimization. The unification of two single three-phase machines in a combined stator results in a reduction of the slots per machine by half. Hence, half the number of turns w available for each machine. With the phase voltage $u_{\mathrm{i,uvw}}$ as a function of w, this results in a reduction of the phase voltages of each individual machine by half.

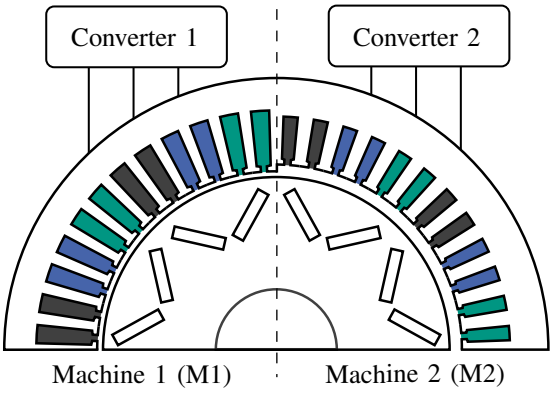

Fig. 1. General topology of SAM with two three-phase systems, fed by two independent converters, supplied by the same DC Link.

The simulation of a coupled model with asymmetric subsystems requires vast computational resources. Hence, two different models for design process are investigated. The level of detail is rather low for a first, separated model and increases for a second, coupled model. The simulation data is derived by using the numerical finite element analysis (FEA) software, Ansys Electronics.

B. Separated model

A three phase PMSM with distributed winding is used as reference machine design (REF) to carry out a design of experiment (DOE). 1000 machines are generated, the stator geometry as well as the air gap is varied. The parameters used in the DOE are illustrated in Fig. 2, named slot height HS, slot width WS, slot opening height HO, slot opening width WO and the air gap δ. The outer stator diameter of each machine must remain constant, compared to the REF.

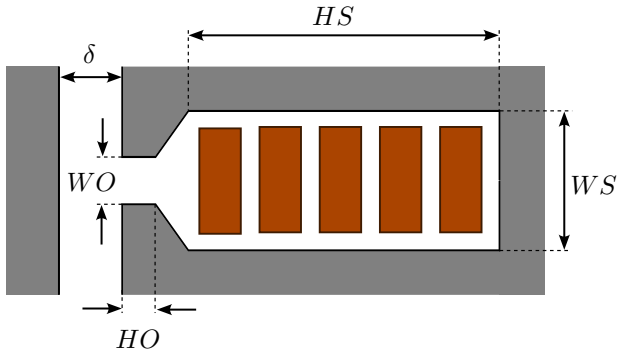

Fig. 2. Modified parameters of the stator slot geometry in DOE, including air gap.

The conductors cross-sectional area is modified proportional to the changes in the slot height and width. The limits used in the geometry variation within the DOE are listed in Tab. I.

Table I
Design parameters - limits and results of the separated model optimization using global optimization algorithm.

Geometric Parameters	**Limits DOE**	**Results optimization**	
	REF	M1	M2
Slot height HS	$\pm$ 25 %	10 %	0 %
Slot width WS	$\pm$ 25 %	5 %	0 %
Slot opening height HO	$\pm$ 25 %	1.5 %	0 %
Slot opening width WO	$\pm$ 25 %	2.5 %	0 %
Airgap δ	$\pm$ 80 %	0 %	66 %

The geometry variation of REF is followed by post-processing algorithms to calculate the copper and iron losses. The magnet losses in the rotor are neglected. With this information, the efficiency maps for each design in the DOE are derived. The generated data is used in an optimization to determine the two most suited machines M1 and M2 for an asymmetric operation. The Worldwide Harmonized Light Vehicles Test Procedure (WLTP) is used as reference cycle for the optimization problem. The majority of OPs occurring in the WLTP are at partial loads, the required torque can be delivered completely by M1 or M2.
The loss-minimal torque distribution x_{dist} between the machines M1 and M2 offers an additional degree of freedom in the optimization and is described in (1).

$$T_{\mathrm{SAM}} = x_{\mathrm{dist}} \cdot T_{\mathrm{M1}} + (1 - x_{\mathrm{dist}}) \cdot T_{\mathrm{M2}} \tag{1}$$

A global optimization algorithm is used to find the loss-optimal torque distribution x_{dist} in the operating range for each machine combination M1 and M2 within the DOE (2).

$$x_{\mathrm{dist}} = \min \; f\left(P_{\mathrm{cu,DC}}, P_{\mathrm{cu,AC}}, P_{\mathrm{fe}}\right) \tag{2}$$

In addition to the minimization of losses, the boundary conditions of reaching the same maximum torque characteristics as well as not exceeding the maximum possible value of losses during operation must be satisfied, compared to the REF. The optimization results in two machine designs M1 and M2 with

the best efficiency over the WLTP. The final parameters of geometric asymmetry are listed in Tab. I. The distribution map for the optimized design is visualized in Fig. 3, presenting the loss optimal distribution of torque between M1 and M2, where the contours show the value of x_{dist}, with larger values representing a torque distribution in favor of M1.

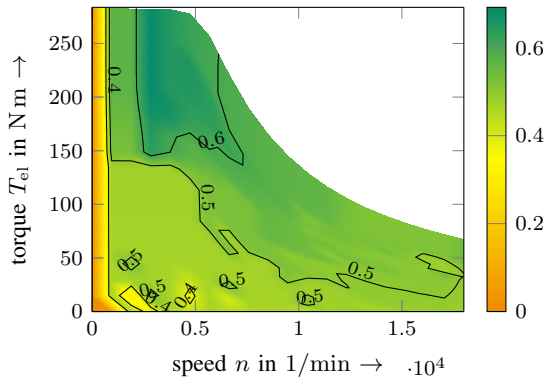

Fig. 3. Loss-optimal distribution map of torque in SAM for asymmetric operation.

Depending on the OP within the operating range, the torque is shifted between M1 and M2. While the operation in favor of M1 is more dominant in the base speed area, the operation of M2 is more efficient at higher speeds in the field weakening area. The geometry of M1 is characterized through a larger value of the parameters HS and WS, compared to REF. The proportional increased conductor area in M1 is responsible for a decreased phase resistance R_{ph1}. This reduces the DC losses (3). Since the DC losses are dominant at the base speed range, it is beneficial to use M1.

$$P_{\mathrm{cu,DC}} = 3 \cdot \left(R_{\mathrm{ph1}} \cdot I_{\mathrm{rms1}}^2 + R_{\mathrm{ph2}} \cdot I_{\mathrm{rms2}}^2 \right) \tag{3}$$

In Fig. 3, this phenomenon is recognizable by a torque distribution $x_{\mathrm{dist}} > 0.5$ for partial loads. In M2, the geometric asymmetry is created by a significant change in the air gap δ, compared to the REF. The operation at high speeds normally requires an increased field weakening negative component in the d-current, which increases the copper losses. The increased air gap of M2 reduces the additional d-current and therefore the copper losses. The general iron losses P_{fe} are described in (4) and depend on the frequency f as well as amplitude of the magnetic flux density B [8]. In the separated model, the iron losses are divided into P_{fe1} and P_{fe2}, due to the DOE and superimposed. In the coupled model, the iron losses P_{fe} depend on the magnetic coupling of all six phases.

$$P_{\mathrm{fe}} = k_{\mathrm{h}} f B^2 + k_{\mathrm{c}} \left(f B \right)^2 + k_{\mathrm{e}} \left(f B \right)^{1.5} \tag{4}$$

The presented iron loss model is calculated by the components of hysteresis, eddy current and excess losses. The iron losses are reduced when the torque is shifted to M2, due to higher magnetic flux densities B in M1, resulting from higher current amplitudes and thinner surface cross-sections in stator teeth and yoke. The distribution map in Fig. 3 reflects this assumption at higher speeds with $x_{\mathrm{dist}} < 0.5$. The total benefit of the separated optimization will be interpreted and discussed in III. The identification of the best suited machine designs with separated optimization results in an asymmetric geometry. The operation is asymmetric as well, due to different loss-optimal OPs of the two individual machines. All magnetic coupling between M1 and M2 is neglected so far and will be taken into account in the following section.

C. Coupled model

Besides the focus on the identification of geometry parameters to maximize the cycle efficiency, the magnetic coupling between the two systems is described. The segmentation of the individual machines leads to abrupt changes in the geometry at the segment boundaries. The operation of the machines M1 and M2 is characterized through different current amplitudes and phase shifts. Both asymmetries combined need further investigation. Hence, a coupled model is simulated using FEA. The magnetic flux linkage Ψ_{i}, $\mathrm{i} = [\mathrm{d1}, \mathrm{q1}, \mathrm{d2}, \mathrm{q2}]$ is described in (5) by a function depending on five dimensions, the d- and q- currents in both systems and the position of the rotor angle γ.

$$f : (i_{\mathrm{d1}}, i_{\mathrm{q1}}, i_{\mathrm{d2}}, i_{\mathrm{q2}}, \gamma) \mapsto (\Psi_{\mathrm{d1}}, \Psi_{\mathrm{q1}}, \Psi_{\mathrm{d2}}, \Psi_{\mathrm{q2}}) \tag{5}$$

The voltage equations for a DTEM in dq-reference frame are presented in (6) and derived from [9]. Due to the presence of additional magnetic coupling terms between the systems (5), the effects on the voltages are investigated.

$$\begin{aligned}
u_{\mathrm{d1}} &= R_{\mathrm{ph1}} \cdot i_{\mathrm{d1}} + \frac{\mathrm{d}\Psi_{\mathrm{d1}}}{\mathrm{d}t} - \omega_{\mathrm{el}} \cdot \Psi_{\mathrm{q1}} \\
u_{\mathrm{q1}} &= R_{\mathrm{ph1}} \cdot i_{\mathrm{q1}} + \frac{\mathrm{d}\Psi_{\mathrm{q1}}}{\mathrm{d}t} + \omega_{\mathrm{el}} \cdot \Psi_{\mathrm{d1}} \\
u_{\mathrm{d2}} &= R_{\mathrm{ph2}} \cdot i_{\mathrm{d2}} + \frac{\mathrm{d}\Psi_{\mathrm{d2}}}{\mathrm{d}t} - \omega_{\mathrm{el}} \cdot \Psi_{\mathrm{q2}} \\
u_{\mathrm{q2}} &= R_{\mathrm{ph2}} \cdot i_{\mathrm{q2}} + \frac{\mathrm{d}\Psi_{\mathrm{q2}}}{\mathrm{d}t} + \omega_{\mathrm{el}} \cdot \Psi_{\mathrm{d2}}
\end{aligned} \tag{6}$$

A graphical visualization of the effects on the voltages over one electrical period is carried out using the voltage space vectors. Hence, the dq-voltages (6) are transformed into the $\alpha\beta$-reference frame. The space vectors of M1, M2, REF as well as the voltage limit are compared and interpreted in III. The electromagnetic torque $T_{\mathrm{el,DTEM}}$ of DTEM is characterized by an interaction between both winding sets [9]. Mathematically, $T_{\mathrm{el,DTEM}}$ is described by (7).

$$T_{\mathrm{el,DTEM}} = \frac{3}{2} p \left(\Psi_{\mathrm{d1}} i_{\mathrm{q1}} - \Psi_{\mathrm{q1}} i_{\mathrm{d1}} + \Psi_{\mathrm{d2}} i_{\mathrm{q2}} - \Psi_{\mathrm{q2}} i_{\mathrm{d2}} \right) \tag{7}$$

The effects of the magnetic coupling on $T_{\mathrm{el,DTEM}}$ are evident and compared using the FEA results. Additional harmonics, average torque and torque-ripple are discussed in detail in III.

III. Results and Discussion

The advantages and disadvantages due to the magnetic coupling in SAM are studied and compared with respect to the electromagnetic torque, the resulting dq-voltages and the overall losses during the WLTP. Due to the geometric and electric asymmetry, additional harmonics in the magnetic flux linkage are present. In faulty condition, DTEM cause additional 2nd and 4th harmonics with respect to the dq-reference frame in the torque and voltage spectrum [5], [10]. The magnitudes of the additional harmonics strongly depend on the operation and torque distribution x_{dist} in SAM.

A. Effects on torque

The effects of the magnetic coupling on the electromagnetic torque are investigated for different operating points and compared between SAM and REF. Figure 4 illustrates the base point of both machines. In Fig. 4(a) the typical 6th harmonic and multiple are visible in the spectrum. The amplitudes are compared in a dB-scale.

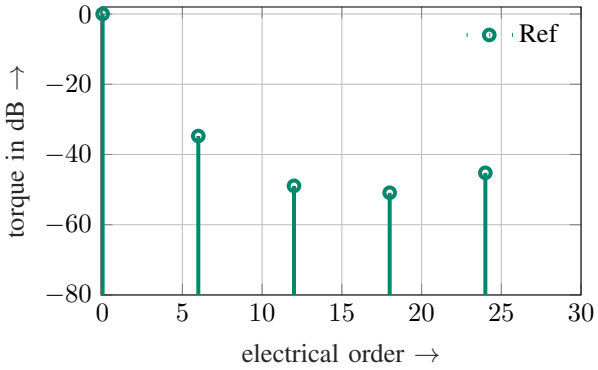

(a) Torque spectrum of REF in base point, compared in dB-scale.

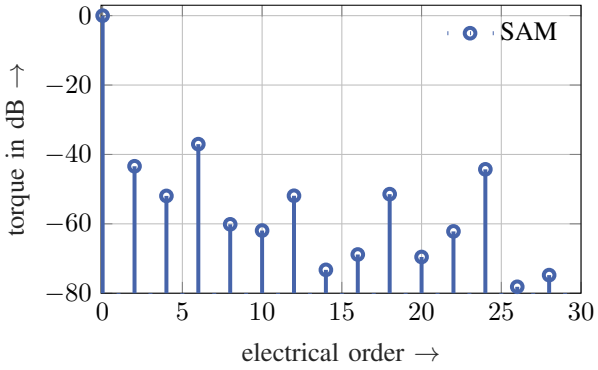

(b) Torque spectrum of SAM in base point, compared in dB-scale.

Fig. 4. Comparison of electromagnetic torque spectrum between REF and SAM in base point.

Compared to REF, additional 2nd and 4th harmonics are evident in the spectrum of SAM, visible in Fig. 4(b). The magnetic coupling between the systems M1 and M2 is mathematically described in (5), (7). Considering the geometric and electric asymmetry of the two systems, the additional harmonics are expected [5], [10]. The SAM is able to deliver the average torque, compared to REF. The torque ripple in general depends on the OP. The amplitudes of the 2nd and 4th harmonics in SAM are lower than the existing 6th harmonic. In addition, the existing harmonics are slightly reduced. These effects result in minor changes in the torque ripple, which slightly in- or decreases, depending on the OP.

B. Effects on induced voltages

The additional 2nd and 4th harmonics in the magnetic flux linkage induce additional voltage harmonics. The voltages of M1 and M2, described in dq-reference frame in (6) are illustrated by space vector trajectories in the $\alpha\beta$-system over one electrical period and presented in Fig. 5. The voltage limits of the two converters are visualized and simplified to an operation without over modulation for initial investigations. Possible critical OPs are identified, if the space vectors of M1 and M2 exceed the voltage limits of the converter.

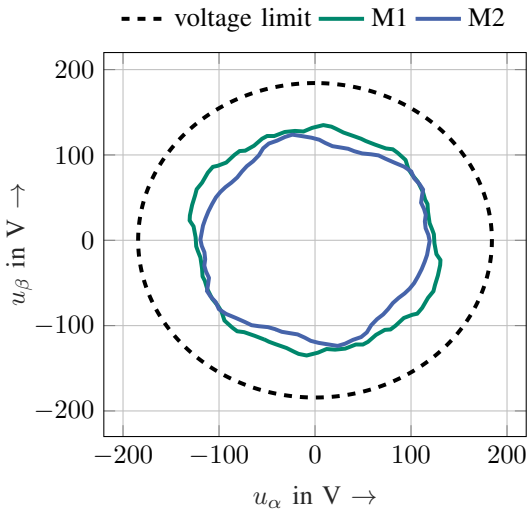

(a) Voltage trajectory for uncritical OP.

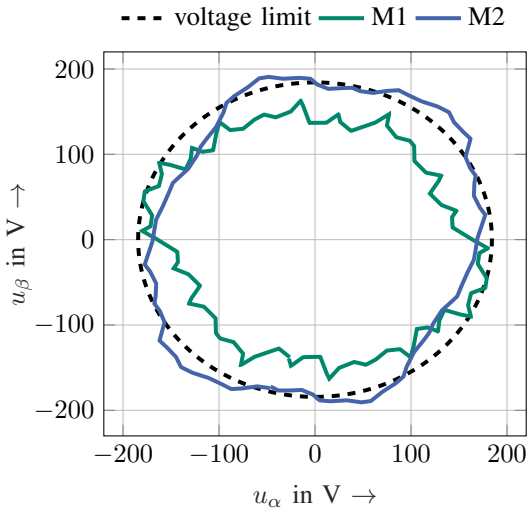

(b) Voltage trajectory for critical OP.

Fig. 5. Voltage trajectories over electrical period for a critical and an uncritical OP within the WLTP.

Figure 5(a) describes an OP within the WLTP at partial loads and low speeds. The asymmetry between the two systems M1 and M2 is visible. The voltage trajectories lie within the voltage limits, hence the OP is reachable. On the contrary, the OP in Fig. 5(b) is characterized by the voltage trajectory of M2 exceeding the voltage limit. The OP visualized lies in the WLTP at high speeds. The asymmetrically induced voltages reach the voltage limit of converter 2 at an earlier stage, the OP is not reachable without further investigation of the magnetic coupling. The voltage trajectories exceeding the maximum limits of the converters demonstrate the importance of considering the magnetic coupling at an earlier stage of the design process. The operation of OP in Fig. 5(b) requires either an additional field weakening negative d-current or a shift of the torque distribution x_{dist} to another OP. Both possibilities will result in a less beneficial operation.

C. Effects on losses in WLTP

The presented design approach focuses on an improved cycle efficiency. The DC and AC copper losses as well as the iron losses are calculated using post-processing algorithms, combined with the magnetic fields taken from the FEA. The additional 2nd and 4th harmonics in the magnetic flux have been discussed in detail. The efficiency map of a coupled model is calculated and the losses during a WLTP cycle are derived. Figure 6 displays the losses within the WLTP-High, the last 316 steps of the cycle at high speeds, respectively. The losses occurring in each OP of the cycle are plotted over the time steps, with the assumption of $1\,\mathrm{sec}$ per OP.

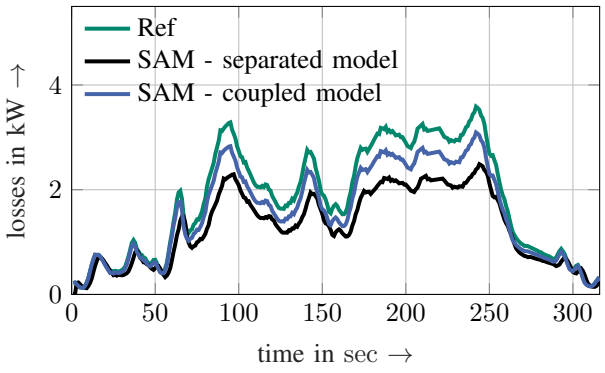

Fig. 6. Overall losses generated over WLTP-High for two variants of control for SAM, compared to a three-phase REF.

In addition to the three-phase REF, two variants of SAM are presented. Both variants are simulated with the same coupled FEA model, but differ in the calculation of the required current pairs for each OP. The separated model is simulated with the distribution map derived in (2), without any knowledge of the magnetic coupling. While neglecting the coupling during the calculation of the voltage limit, the overall losses during the WLTP can be reduced by $9.1\,\%$. The losses of the coupled model are calculated with consideration of the simplified voltage limits of both converters. Considering the coupling in the voltage limits, the loss reduction decreases to $3.6\,\%$ in the WLTP, compared to REF.

IV. Conclusion

A. Summary

A new approach of segmented DTEM with asymmetric operation is presented in this paper. The torque in each OP within the operating range is loss-optimal distributed to two independently fed machines M1 and M2. Two models are introduced, at first a separated approach to find the optimal design parameters as well as an optimal torque distribution between the two individual systems. The second model is a detailed coupled model, which considers the magnetic coupling between the two asymmetric systems. The coupling results in additional 2nd and 4th harmonics in the flux linkages. The effects of magnetic coupling are evaluated regarding the average torque and ripple, the losses during operation and the induced voltages within the two systems. The average torque is accessible and the additional ripple in tangential direction is negligible compared to a REF. The induced voltages limit the operating range and reduce the potential to improve the cycle efficiency of SAM. Without further optimization of the overall system, the advantages in the WLTP are $3.6\,\%$. Theoretically, $9.1\,\%$ within the cycle are possible, if the magnetic coupling is reduced significantly.

B. Outlook

The future research will focus on effective control strategies for DTEM with asymmetric designs, as well as possibilities to reduce the undesired magnetic coupling through different geometry optimization and alternative winding arrangements. With these researches, the theoretical potential of $9.1\,\%$ is intended to be reached. The separated design optimization will be improved using semi-analytical models to describe the magnetic coupling at an earlier state of the design process. Noise, vibration and harshness, due to radial forces, will be taken into account. Also, the thermal behavior in asymmetric operation will be investigated.

References

[1] L. Parsa, "On advantages of multi-phase machines," in *31st Annual Conference of IEEE Industrial Electronics Society, 2005. IECON 2005*, 2005, p. 6 pp.

[2] T. Miller and M. I. McGilp, "Analysis of multi-phase permanent-magnet synchronous machines," in *2009 International Conference on Electrical Machines and Systems*. Piscataway, NJ: IEEE, 2009, pp. 1–6.

[3] S. Foitzik and M. Doppelbauer, "Fault Tolerant Control by Asymmetric Operation of Double Three-Phase PMSMs with Inter-Turn Faults," in *2020 International Conference on Electrical Machines (ICEM)*, 2020, pp. 1342–1348.

[4] L. Alberti and N. Bianchi, "Impact of winding arrangement in dual 3-phase induction motor for fault tolerant applications," in *The XIX International Conference on Electrical Machines - ICEM 2010*, 2010, pp. 1–6.

[5] C. Babetto, N. Bianchi, A. Torreggiani, C. Bianchini, M. Davoli, and A. Bellini, "Optimal Design and Experimental Validation of a Synchronous Reluctance Machine for Fault-Tolerant Applications," in *ECCE 2019*. Piscataway, NJ: IEEE, 2019, pp. 4880–4887.

[6] C. Babetto and N. Bianchi, "C. Babetto; N. Bianchi - Synchronous Reluctance Motor with Dual Three-Phase Winding for Fault- Tolerant Applications," in *2020 International Conference on Electrical Machines (ICEM)*, 2020, pp. 2297–2303.

[7] C. Babetto, N. Bianchi, A. Torreggiani, C. Bianchini, M. Davoli, and A. Bellini, "Design Optimization and Analysis of a Synchronous Reluctance Machine for Fault-Tolerant Applications," in *2019 IEEE International Electric Machines & Drives Conference (IEMDC)*, 2019, pp. 1784–1791.

[8] D. Lin, P. Zhou, W. N. Fu, Z. Badics, and Z. J. Cendes, "A Dynamic Core Loss Model for Soft Ferromagnetic and Power Ferrite Materials in Transient Finite Element Analysis," *IEEE Transactions on Magnetics*, vol. 40, no. 2, pp. 1318–1321, 2004.

[9] J. Karttunen, S. Kallio, P. Peltoniemi, P. Silventoinen, and O. Pyrhönen, "Dual three-phase permanent magnet synchronous machine supplied by two independent voltage source inverters," in *International Symposium on Power Electronics Power Electronics, Electrical Drives, Automation and Motion*, 2012, pp. 741–747.

[10] S. Foitzik and M. Doppelbauer, "Analytical Model of a Six-Phase PMSM for the Simulation of Stator Winding Faults on Turn Level," in *2019 IEEE International Electric Machines & Drives Conference (IEMDC)*. IEEE, 5/12/2019 - 5/15/2019, pp. 185–191.